Applied-Field Topology Effects on the Thrust of an MPDT

IEPC-2017-182

Presented at the 35th International Electric Propulsion Conference
Georgia Institute of Technology · Atlanta, Georgia · USA
October 8–12, 2017

William J. Coogan* and Edgar Y. Choueiri†
Electric Propulsion and Plasma Dynamics Lab
Princeton University, Princeton, NJ, 08544, USA

The effects of applied-field topology on the thrust of applied-field magnetoplasmadynamic thrusters are investigated. While it has been previously shown that thrust depends linearly on the anode radius, this radius has not been well-defined, and the prevalence of diverging anodes makes it important to determine which radius should be applied to a thrust calculation. The applied-field topology plays a key role in determining this radius, since the magnetic field can generate a pressure confining the plasma within a certain boundary. Because the gasdynamic pressure pushes against this boundary, this work seeks to determine how the ratio of the two pressures determines the effective anode radius. In order to make this determination, two different applied-field topologies are tested—one contoured to the anode, and one which diverges more slowly than the anode. The mass flow rate is varied in order to change the gasdynamic pressure while the parameters affecting the magnetic pressure are held fixed. The resulting change in force on the solenoid, corresponding to the change in the applied-field component thrust, is measured. It is found that the effective anode radius changes by as much as a factor of two when the anode expands more rapidly than the magnetic field, but is nearly constant when the anode is contoured to the magnetic field.

Nomenclature

B_A	Applied magnetic field, T
$\boldsymbol{\mathcal{B}}$	Maxwell stress tensor
F	Force, N
J	Current, A
k	Thrust coefficient
k_B	Boltzmann constant, J/K
l	Axial length, m
$\dot{m}$	Mass flow rate, kg/s
M	Atomic mass, u
n	Density, m^{-3}
$\hat{\mathbf{n}}$	Unit normal
N_A	Avogadro's number
p	Pressure, Pa
r	Radius, m
r_B	Average solenoid radius, m
T	Thrust, N
$\mathcal{T}$	Temperature, K
z	Distance from solenoid along thrust axis
α	Angle of magnetic field with respect to thrust axis
β	Ratio of gasdynamic to magnetic pressure
κ	Effective anode radius scaling parameter
μ_0	Permeability of free space, $\mathrm{N/A}^2$
ξ	Steepness of logistic function
ν_ei	Electron-ion collision frequency, s^{-1}
$\bar{\Phi}$	Contour of anode to magnetic field

Subscripts

a	Anode
a0	Anode throat or backplate
ae	Anode exit plane
AF	Applied-field
B	Magnetic
GD	Gasdynamic

*Graduate Student, MAE Dept., wcoogan@princeton.edu
†Chief Scientist, EPPDyL, Professor, Applied Physics Group, MAE Dept., choueiri@princeton.edu

H	Hall-effect component	Φ	With respect to surface of constant magnetic flux
i	Ion		
r	Radial direction		
θ	Azimuthal direction		

I. Introduction

Since the 1960s, the applied-field magnetoplasmadynamic thruster (AF-MPDT) has proven to be a high-thrust density alternative to other forms of electric propulsion.[1] Although the power requirements for this thruster have made it an infeasible option for space exploration up until the present, the projection for as much as 200 kW of solar power for spacecraft[2,3] may make AF-MPDT operation possible in the near- to mid-term. However, questions remain as to how to optimize the performance of this thruster for the requirements of a given mission. A useful tool for this optimization would be a model with which to predict the thrust over a large and varied parameter space.

The thrust of an AF-MPDT is typically assumed to be the sum of the applied-field, self-field, and gasdynamic thrust components.[4–9] We previously showed[10] that when the applied-field thrust component is dominant, the thrust is proportional to the current, the applied-field strength, and an electrode radius which is determined by the contours of the anode and applied field, as well as by the ratio of gasdynamic to magnetic pressure.

While our previous method for determining the parameters affecting thrust was statistical in nature, we now provide direct experimental evidence of the effects of applied-field topology and the plasma beta parameter on thrust. We directly measure changes in the applied-field component of the thrust while varying the mass flow rate when all other parameters are held fixed and the applied-field is contoured to the anode. We then repeat this experiment with a magnetic field that diverges more slowly than the anode. The changing mass flow rate serves to change the plasma beta parameter, and we show how this change affects the thrust for each of the two applied-field configurations. In addition to our experiment, we use the thrust data of three AF-MPDTs in the literature, which have rapidly expanding anodes, to show that the dependence of thrust on the plasma beta parameter is not unique to our thruster.

In Sec. II, we outline the scenarios in which the applied-field thrust model of Tikhonov et al. fails to predict measurement, and provide a theoretical model for the upper and lower bounds of the thrust for such cases. We give an overview of our experimental setup in Sec. III, followed by the results of our experiment in Sec. IV.

II. Theory

The application of an axial, diverging magnetic field to an MPDT (Fig. 1a) produces a Lorentz force that swirls the plasma. As the plasma expands through the diverging magnetic field, this rotating motion is redirected along the field lines, which, assuming the plasma subsequently detaches from the magnetic field lines, generates thrust. Due to the collisional nature of MPDTs, the swirling motion also results in an azimuthal Hall current. This Hall current crossed with the radial component of the magnetic field generates additional thrust. The combination of these acceleration mechanisms forms the applied-field thrust component.

Tikhonov et al. showed that the applied-field component of the thrust from an AF-MPDT can be expressed as[11]

$$T_{\mathrm{AF}} = kJB_{\mathrm{A}}r_{\mathrm{a}} \tag{1}$$

where k is a scaling constant, J is the current, B_{A} is the applied field strength, and r_{a} is the effective anode radius. While they provide an explicit expression for the scaling constant in terms of the length of the cathode and the magnetic flux at two axial positions within the anode, the inverse dependence on cathode length makes the expression unsuitable for thrusters with recessed cathodes. Tikhonov et al. give a value[4,8,12–14] of $k \simeq 0.2$ and note that k can be experimentally determined for any given thruster.

In Ref. 10, we showed that k can be assumed to be 0.14 for all thrusters, and that the variation in thrust for different thrusters is actually due to how the effective anode radius is evaluated. We showed the thrust data in the literature to be better predicted by

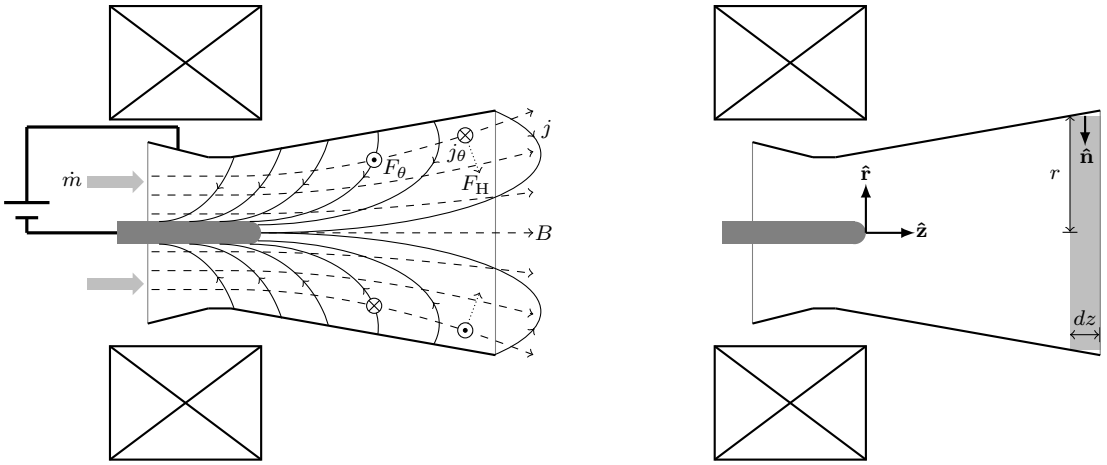

(a) Applied-field Lorentz force **(b) Control volume**

Figure 1: Lorentz forces resulting from an external magnetic field (a) shown in a schematic cross-section of an AF-MPDT. The external magnetic field results in azimuthal and Hall-effect forces (F_θ and F_{H} respectively). The control volume (b) for the calculation of the plasma beta parameter is shown in light gray.

$$T_{\mathrm{AF}} = kJB_{\mathrm{A}}r_{\mathrm{a}}\bar{\Phi}^{-0.13} \tag{2}$$

than by Eq. 1. $\bar{\Phi}$ is the nondimensional value

$$\bar{\Phi} = \frac{r_{\mathrm{ae}}^2 r_{\mathrm{B}}^3}{r_{\mathrm{a0}}^2\left(r_{\mathrm{B}}^2 + l_{\mathrm{a}}^2\right)^{3/2}}, \tag{3}$$

where r_{a0} and r_{ae} are the radii of the anode at the throat and exit plane respectively, r_{B} is the average solenoid radius, and l_{a} is the length of the anode between the throat and the exit plane. $\bar{\Phi}$ is the ratio of the magnetic flux through the exit plane of the anode to the flux through the anode throat and serves as a measure of how well an anode is contoured to the topology of the magnetic field. Equation 3 is found using the Biot-Savart law for a solenoid (Eq. 13) with the assumption that the solenoid does not extend beyond the anode throat. A perfectly contoured anode yields $\bar{\Phi} = 1$, while an anode that expands more rapidly than the magnetic field yields $\bar{\Phi} > 1$. We demonstrated that when $\bar{\Phi} \leq 1$, Eq. 1 most closely predicts measurement when $r_{\mathrm{a}} = r_{\mathrm{ae}}$. However, when $\bar{\Phi} > 1$, the same expression overpredicts the data. We attribute this overprediction to the freezing of the plasma to the magnetic field lines. A frozen plasma will not expand radially across magnetic field lines, and so the volume on which the Lorentz force acts may be less than the anode volume when $\bar{\Phi} > 1$. We therefore assert that the effective anode radius is less than r_{ae} when $\bar{\Phi}$ is large.

We now seek an analytical expression for the effective anode radius. Based on the observations of thrust with respect to $\bar{\Phi}$, we assume that $r_{\text{ae-}\Phi} \leq r_{\mathrm{a}} \leq r_{\mathrm{ae}}$, where $r_{\text{ae-}\Phi}$ is the radius at which the magnetic flux through the anode exit plane is equal to the flux through the anode throat, as is illustrated in Fig. 2. Substituting $r_{\text{ae-}\Phi}$ for r_{ae} in Eq. 3 and solving for the case when $\bar{\Phi} = 1$ yields

$$r_{\text{ae-}\Phi} = r_{\mathrm{a0}}\left(\frac{r_{\mathrm{B}}^2 + l_{\mathrm{a}}^2}{r_{\mathrm{B}}^2}\right)^{3/4}. \tag{4}$$

We can express r_{a} as

$$r_{\mathrm{a}} = r_{\text{ae-}\Phi} + \kappa\left(r_{\mathrm{ae}} - r_{\text{ae-}\Phi}\right), \tag{5}$$

where κ is a scaling parameter such that $0 \leq \kappa \leq 1$. We expect this parameter to be a function of the degree to which the plasma is frozen to the magnetic field. κ will therefore have largest values when the gasdynamic pressure is large compared to the magnetic pressure. We assume that

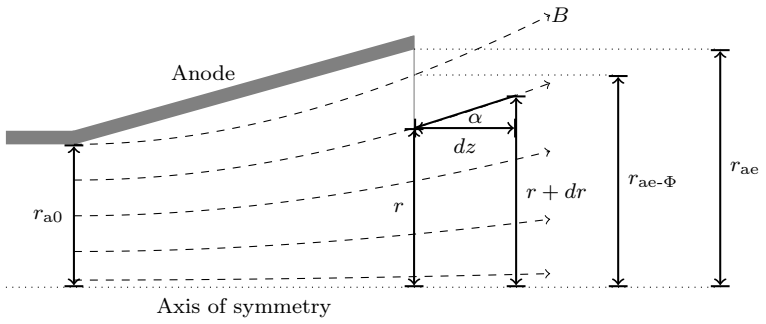

Figure 2: Geometry for determining the various length scales from the magnetic field.

$$\kappa = f\left(\beta_{\mathrm{ae}}\right), \tag{6}$$

where β_{ae} is the ratio of gasdynamic to magnetic pressure at the anode exit plane. κ can be determined experimentally using thrust measurements in which the applied-field thrust component is dominant by rearranging Eqs. 1, 4, and 5 to obtain the relation

$$\kappa = \left(\frac{T}{kJB_{\mathrm{A}}} - r_{\text{ae-}\Phi}\right)\left(r_{\mathrm{ae}} - r_{\text{ae-}\Phi}\right)^{-1}. \tag{7}$$

In order to experimentally determine the dependence of κ on β_{ae}, we require an analytical expression for β_{ae}. We assume that the plasma is fully ionized and that the gasdynamic pressure at the exit plane, p_{GD}, is isotropic. This pressure is given by the ideal gas equation for ions:

$$p_{\mathrm{GD}} = n_{\mathrm{i}} k_{\mathrm{B}} \mathcal{T}_{\mathrm{i}}, \tag{8}$$

where n_{i} is the ion density, k_{B} is the Boltzmann constant, and $\mathcal{T}_{\mathrm{i}}$ is the ion temperature. We assume that $\mathcal{T}_{\mathrm{i}} = 2$ eV, which is on the order of temperatures found in AF-MPDTs.[8,15–18]

Assuming that all ions pass through the exit plane within the effective radius, and that the density within this radius is constant, the density is given by

$$n_{\mathrm{i}} = \frac{1000\dot{m}^2 N_{\mathrm{A}}}{\pi r_{\mathrm{a}}^2 M T}, \tag{9}$$

where $\dot{m}$ is the mass flow rate, N_{A} is Avogadro's number, M is the atomic mass, and T is the total thrust. We assume the applied-field thrust component to be dominant, so that $T \simeq T_{\mathrm{AF}}$ and can be calculated using Eq. 1 for a given r_{a}.

The magnetic pressure is

$$\mathbf{p}_B = \boldsymbol{\mathcal{B}} \cdot \hat{\mathbf{n}}, \tag{10}$$

where $\boldsymbol{\mathcal{B}}$ is the Maxwell stress tensor and $\hat{\mathbf{n}}$ is the unit normal vector for the surface of interest. The components of the Maxwell stress tensor are[19]

$$\mathcal{B}_{ij} = \frac{1}{\mu_0} B_i B_j - \frac{1}{2\mu_0} B^2 \delta_{ij}. \tag{11}$$

The surface of interest is the interior of a cylinder at the anode exit plane (illustrated in Fig. 1b), and so the unit normal vector in cylindrical coordinates is $(-1, 0, 0)$. The magnetic pressure towards the thrust axis is then

$$p_B = \frac{1}{\mu_0}\left(\frac{1}{2}B^2 - B_r^2\right), \tag{12}$$

where B_r is the radial component of the magnetic field. The magnitude of B is found using the Biot-Savart law for a solenoid,

$$B(z) = B_{\mathrm{a0}} \frac{r_{\mathrm{B}}^3}{\left(r_{\mathrm{B}}^2 + z^2\right)^{3/2}}, \tag{13}$$

where z is the axial distance from the solenoid to the anode exit plane and B_{a0} is the magnetic field strength inside the solenoid.

We determine B_r at the exit plane for a given r by first solving for the magnetic field strength a distance dz beyond the exit plane (again using Eq. 13). Then, we find the radius $r + dr$ at which the flux through the plane at $z + dz$ is equivalent to the flux through the exit plane within r, as is illustrated in Fig. 2. We must solve

$$\pi r^2 B(z) = \pi (r + dr)^2 B(z + dz) \tag{14}$$

in order to determine the angle α of the magnetic field with respect to the thrust axis at (r, z):

$$\alpha = \tan^{-1}\left(\frac{dr}{dz}\right). \tag{15}$$

While there is no simple expression for $\frac{dr}{dz}$, dr is easy to compute for an arbitrarily small dz and for a given solenoid dimension. We use $dz = 0.1$ mm for all calculations. The radial component of the magnetic field is given by

$$B_r = B \sin(\alpha). \tag{16}$$

Combining Eqs. 8, 9, and 12–16 gives the solution to

$$\beta_{\mathrm{ae}}(r) = \frac{p_{\mathrm{GD}}}{p_B}. \tag{17}$$

Because we expect κ to depend on the degree to which the plasma is frozen, we evaluate β_{ae} for the case where $r = r_{\mathrm{a}} = r_{\mathrm{ae\text{-}\Phi}}$.

We now require a function which scales κ from 0 to 1 for any value of β_{ae}. Because β_{ae} will span a number of orders of magnitude, we take $\ln(\beta_{\mathrm{ae}})$ to be the variable. We impose that $\kappa \to 0$ as $\ln(\beta_{\mathrm{ae}}) \to -\infty$ and $\kappa \to 1$ as $\ln(\beta_{\mathrm{ae}}) \to \infty$, which leads to a function that asymptotes to 0 and 1 at the respective limits of $\ln(\beta_{\mathrm{ae}})$. The logistic function serves this purpose well, and so we assume the general form

$$\kappa(\beta_{\mathrm{ae}}) = \frac{1}{1 + e^{-\xi[\ln(\beta_{\mathrm{ae}}) - \ln(\beta_{\mathrm{ae\text{-}0}})]}}, \tag{18}$$

where ξ is the steepness of the curve and $\beta_{\mathrm{ae\text{-}0}}$ is the value of β_{ae} for which $\kappa = 0.5$ and the curvature of κ changes signs. We determine ξ and $\ln(\beta_{\mathrm{ae\text{-}0}})$ by using a χ^2 test for goodness of fit, weighting each κ value by the inverse of the square of the error on that value. The error on κ is determined by propagating the thrust measurement error.

III. Experimental Setup

In order to experimentally verify the predicted effects of β_{ae} on thrust, and to determine if these effects are exclusive to thrusters for which $\bar{\Phi} > 1$, we have designed an experiment with which both β_{ae} and $\bar{\Phi}$ can be independently controlled.

A. Argon Lorentz Force Accelerator

The argon Lorentz force accelerator (ALFA), which is shown schematically in Fig. 3, is an argon-fed AF-MPDT that was constructed in 2017 in the Electric Propulsion and Plasma Dynamics Laboratory. Both the cathode and anode are made from AXM-5Q POCO® graphite. All propellant is injected through the orificed hollow cathode, which contains a lanthanum hexaboride (LaB_6) emitter.

When the solenoid is positioned as shown in Fig. 3, the anode interior is contoured to the topology of the magnetic field. However, the solenoid can be moved along the thrust axis as shown in Figs. 4a and b so that the anode diverges more rapidly than the magnetic field, providing larger $\bar{\Phi}$ values. All data from the ALFA were gathered in these two configurations, which we will refer to as contoured (Fig. 4a) and constricted

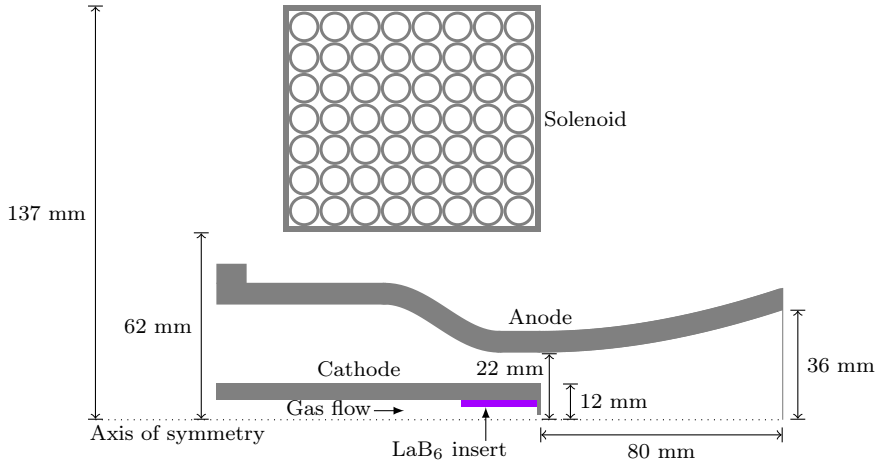

Figure 3: Cross-section of the ALFA, which is symmetric about the thrust axis.

(Fig. 4b) applied-field configurations. In the constricted applied-field configuration, we determine $r_{\text{ae-}\Phi}$ by replacing l_{a} in Eq. 4 with the distance from the end of solenoid to the anode exit plane z, since the magnetic field only expands over the latter distance. This configuration yields $r_{\text{ae}}/r_{\text{ae-}\Phi} = 1.5$.

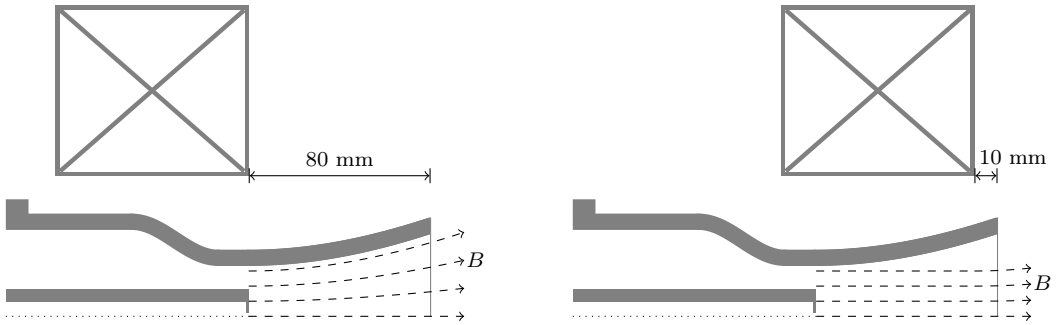

(a) Anode contoured to applied field **(b) Constricted applied field**

Figure 4: Contoured (a) and constricted (b) configurations and the corresponding applied-field topologies.

B. Thrust Stand

The thrust stand, which is illustrated in Fig. 5 and described in Ref. 20, is an inverted pendulum that supports only the solenoid. Because the applied-field component of the thrust exerts an equal and opposite force on the solenoid, a calibrated measurement of the deflection of the solenoid can be used to determine T_{AF}.

C. Method

Because $\beta_{\text{ae}} \propto \dot{m}^2$, we measure how thrust changes as a function of $\dot{m}$ for both the contoured and constricted magnetic field topologies and for a range of different J values. For a given J, we test only two $\dot{m}$ values: one high and one low. In order to consistently change the mass flow rate between these two values, we have implemented a new mass flow control system. This system is composed of two sonic orifices, which run in parallel, and which are toggled on and off using ball valves. When both valves are open, the mass flow rate is high, and when one is closed, the flow rate is low. The mass flow rate is recorded using an OMEGA® FMA-A2404 flow meter.

A measurement of T_{AF} requires accounting for the electromagnetic tare forces between the thrust stand and external current-carrying components. In order to remove this tare force from the total force measurement, we must repeat each measurement for a given set of operating parameters with the current through the solenoid reversed. Because the tare force is equal in magnitude, but in the opposite direction with respect to T_{AF}, averaging the two measurements yields T_{AF}. However, this calculated thrust includes an error from each force measurement. Because we are primarily interested in whether or not there is a *change* in T_{AF} (ΔT_{AF}) resulting from a change in $\dot{m}$, and because the electromagnetic tare force is constant regardless of the value of $\dot{m}$, we instead measure ΔT_{AF} for a given change in $\dot{m}$, eliminating one source of measurement error.

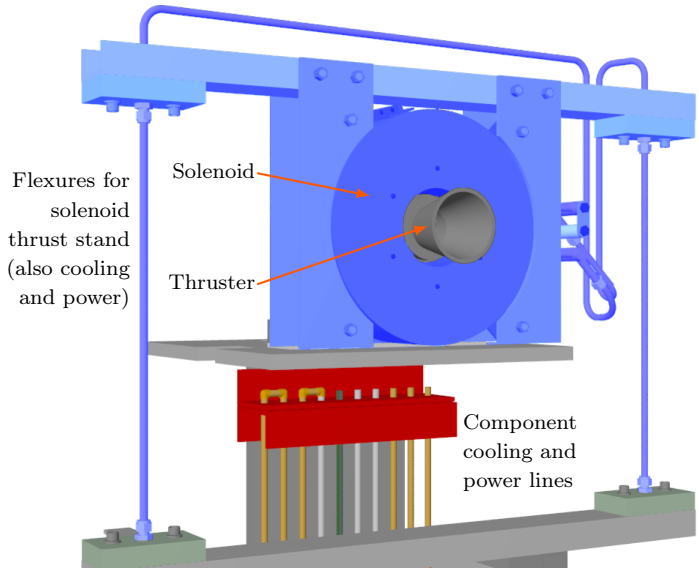

Figure 5: Schematic of the solenoid thrust stand for measurement of the applied-field component of the thrust. Moving components are shown in blue.

The deflection of the thrust stand is measured using a Macro Sensors PR 750-100 linear variable displacement transformer (LVDT), which has a sensitivity of 155 mV/V/mm. In addition, a General Electric model 3300 8MM proximitor duplicates this measurement. The proximitor has a limited range compared to the LVDT, but provides an order of magnitude greater resolution. In order to keep the proximitor within range of the thrust stand, its position can be adjusted while firing by use of a translation stage. While this motion is unsuitable to a measurement of T_{AF}, ΔT_{AF} can be measured once the proximitor is at rest.

Calibration is performed in situ by applying a known force along the thrust axis and measuring the deflection. At least three different forces are tested to ensure linearity between force and measured voltage.

IV. Results

A. Data from the Literature

In addition to using applied-field thrust component measurements made with the ALFA in order to determine κ, we can use existing thrust data as long as certain criteria are met. Although most thrust measurements in the literature are of the total thrust, we can apply the same method used in Ref. 10 to determine if the applied-field thrust component is a significant percentage of the total thrust. We assume that if the thrust predicted by Eq. 1 is greater than 90% of the measured thrust, then the measurement is approximately one of T_{AF}. We are also limited to data taken at background pressures ≤ 1 mTorr, as pressures exceeding this value have been shown to affect thrust.[10]

We further limit the data available in the literature to that for which $\bar{\Phi} > 1$. The AF-MPDT database[23] contains three thrusters meeting our requirements, the relevant parameters for each of which are given in Table 1. These thrusters have large $r_{\mathrm{ae}}/r_{\mathrm{ae\text{-}\Phi}}$ values, and so we expect T_{AF} to change substantially as a

Table 1: Thrusters used in analysis.

Thruster	$r_{ae}/r_{ae\text{-}\Phi}$	Propellant	Typical $\ln(\beta_{ae})$	$\ln(\beta_{ae\text{-}0})$	Reference
H2-4F	4.74	H_2	-6.0 to -4.3	-3.9	21
X2C-Rad	3.92	Li	-8.5 to -3.0	-6.7	22
X2C-H20	3.92	Cs	-9.0 to -6.6	-9.3	22

function of $\ln(\beta_{ae})$.

Thrust measurement error was not reported for the H2-4F thruster. In order to lessen the bias on our conclusions by the data for this thruster, we assume the error to be 15% of the measurement. This percentage is the largest reported error for data taken at less than 1 mTorr and for which Eq. 1 predicts greater than 90% of the measurement.

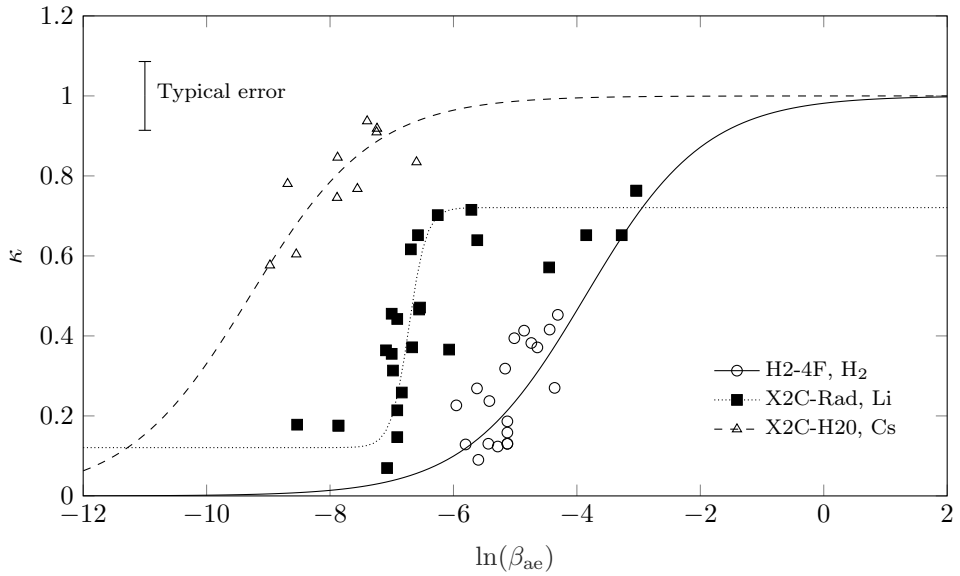

Figure 6: κ as a function of $\ln(\beta_{ae})$ for the H2-4F, X2C-Rad, and X2C-H20 thrusters along with the fit to the data for each.

Figure 6 shows κ as a function of $\ln(\beta_{ae})$. We see that the data is within the range of $0 \leq \kappa \leq 1$ and that κ generally increases with increasing $\ln(\beta_{ae})$. However, the β_{ae} value for the inflection point for each thruster differs by orders of magnitude. Since two of the thrusters, the X2C-Rad and the X2C-H20, are geometrically identical, and differ only in the anode cooling mechanism and propellant species used, we conclude that we have not captured the dependence of κ on propellant species.

While the behavior of κ is generally described by a logistic function ranging from 0 to 1, the κ values for the X2C-Rad reach horizontal asymptotes at $\kappa = 0.12$ and $\kappa = 0.72$. In order to capture this observed behavior, we allowed the upper and lower limits of the logistic function to vary while solving for the fit function. There is a sharp increase in κ values in the range of $-7.5 < \ln(\beta_{ae}) < -6.5$. Because $\beta_{ae} \propto \dot{m}^2/J$, this sharp increase indicates that for certain thruster geometries and operating conditions, T may have a stronger dependence on $\dot{m}$ than on J.

B. Direct Applied-Field Measurements

We operated the ALFA with an applied field strength of 500 G. The current ranged from 50 to 220 A. The argon mass flow rate was alternated between 2.5 and 5.3 mg/s for each current tested and for each solenoid configuration. The results of our tests for a change in thrust resulting from a change in mass flow rate are shown in Fig. 7. A positive ΔT_{AF} value means that the thrust increased when the mass flow rate was

increased, or decreased when the mass flow rate was decreased. All measurements were taken at background pressures less than 0.3 mTorr.

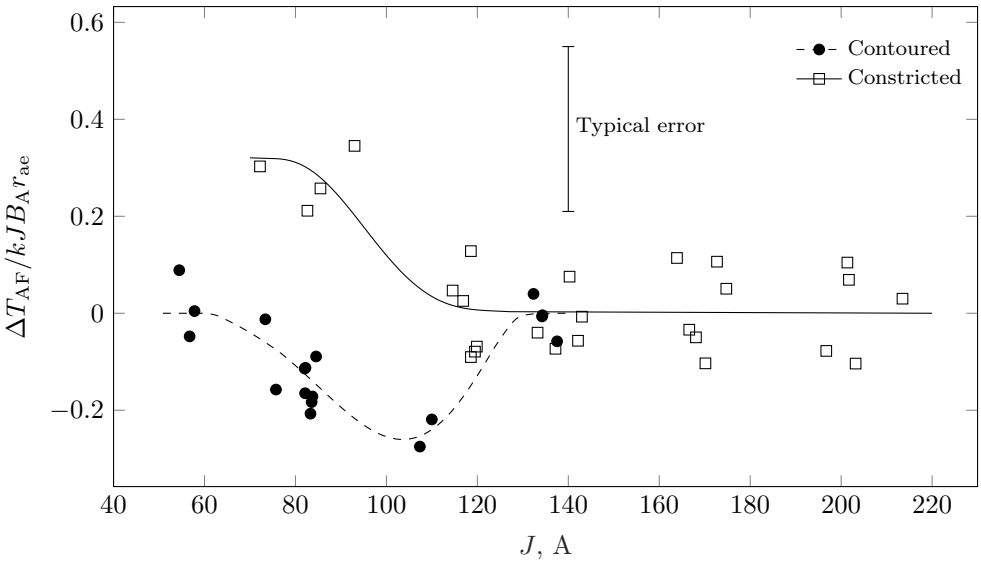

Figure 7: Change in T_{AF} as a fraction of the applied-field thrust predicted by Eq. 1 resulting from a change in $\dot{m}$ from 2.5 to 5.3 mg/s as a function of current.

We see that the measured changes in thrust resulting from a change in mass flow rate are typically a small fraction of the predicted applied-field thrust generated. However, below 120 A, we see a different behavior for each magnetic field configuration. In the constricted applied-field configuration, the applied-field thrust increases with increasing mass flow rate, which is consistent with the prediction made in Sec. II. The maximum $\Delta T_{\mathrm{AF}}/kJB_{\mathrm{A}}r_{\mathrm{ae}}$ value of 0.35 is below the maximum fractional change of 0.5 predicted by the $r_{\mathrm{ae}}/r_{\mathrm{ae\text{-}\Phi}}$ value.

The change in thrust for the contoured magnetic field configuration is either 0 or negative. The negative values are not predicted by our model, but may result from an effect observed in Refs. 10, 21, 24 and 25, where thrust was deteriorated at high facility pressures due to collisions in the plume that interfere with the expansion through the magnetic nozzle.[26–28] A high pressure at the exit of the anode resulting from high $\dot{m}$ can similarly interfere with this expansion.

Using Eq. 7, we convert each ΔT_{AF} measurement to one of $\Delta\kappa$. Then, using Eq. 18, we calculate $\Delta\kappa$ for the ξ and $\ln(\beta_{\mathrm{ae\text{-}0}})$ values that best fit the data. We find that $\ln(\beta_{\mathrm{ae\text{-}0}}) = -5.1$, which is in the range of values given in Table 1. However, this value indicates that $\ln(\beta_{\mathrm{ae\text{-}0}})$ does not monotonically decrease with atomic mass, or increase with ionization energy, as was suggested by the literature data.

V. Conclusion

We have demonstrated that under certain conditions, the applied-field component of the thrust from an AF-MPDT is sensitive to mass flow rate. In some cases, our findings indicate that this thrust component depends more strongly on mass flow rate than on current. We showed that when the anode diverges more rapidly than the magnetic field, the measured thrust is less than that predicted by the model of Tikhonov et al. and attributed this discrepancy to the confinement of the plasma to a volume smaller than that enclosed by the anode. However, we also showed—using data from four different thrusters—that this volume can be increased to the volume of the anode by increasing the ratio of gasdynamic to magnetic pressures. Because $T_{\mathrm{AF}} \propto r_{\mathrm{a}}$ and because we have shown that an anode which expands more rapidly than the magnetic field results in $r_{\mathrm{a}} \leq r_{\mathrm{ae}}$, we conclude that a logical design criteria for AF-MPDTs is that $\bar{\Phi} \leq 1$, so that $r_{\mathrm{a}} = r_{\mathrm{ae}}$.

Acknowledgments

This research was carried out with support from the Program in Plasma Science and Technology through the Princeton Plasma Physics Laboratory. We are grateful to Jack Hollingsworth for all of his assistance in the design and fabrication of the ALFA.

References

[1]G. Kruelle. Characteristics and local analysis of MPD thruster operation. In *AIAA Electric Propulsion and Plasmadynamics Conference*, AIAA-67-672, Colorado Springs, CO, Sept. 11–13, 1967. doi:10.2514/6.1967-672.

[2]D. Brown, B. Beal, and J. Haas. Air Force Research Laboratory high power electric propulsion technology development. Technical report, IEEEAC, 2009.

[3]E. Musk. Spacex interplanetary transport system. URL: http://www.spacex.com/mars.

[4]V. Tikhonov, S. Semenikhin, J. R. Brophy, and J. E. Polk. The experimental performances of the 100 kW Li MPD thruster with external magnetic field. In *24th International Electric Propulsion Conference*, IEPC-95-105, Moscow, Russia, Sept. 19–23, 1995.

[5]G. Herdrich, A. Boxberger, D. Petkow, R. A. Gabrielli, S. Fasoulas, M. Andrenucci, R. Albertoni, F. Paganucci, and P. Rosetti. Advanced scaling model for simplified thrust and power scaling of an applied-field magnetoplasmadynamic thruster. In *46th AIAA/ASME/SAE/ASEE Joint Propulsion Conference*, AIAA-2010-6531, Nashville, TN, July 25–28, 2010. doi:10.2514/6.2010-6531.

[6]L. K. Rudolph. *The MPD Thruster Onset Current Performance Limitation*. PhD thesis, Princeton University, Sept. 1980.

[7]А. Г. Попов and С. А. Семенихин. Расчет Тяги Торцевого Холловского Ускорителя (calculation of thrust for the end-Hall effect rocket). In *VII Всесоюзная Конференция по Плазменным Ускорителям и Ионным Инжекторам (7th Soviet Conference for Plasma Rockets and Ion Injectors)*, pp. 202-203, Kharkiv, Ukraine, Sept. 26–28, 1989.

[8]G. Popov, V. Kim, T. Tikhonov, S. Semenikhin, and M. Tibrina. The third quarterly report on the stages ## 5-6 of the contract on the research studies no. NASA-4851 between RIAME MAI and NASA. Technical Report NASW-4851, RIAME MAI, June 1995.

[9]R. Albertoni, F. Paganucci, and M. Andrenucci. A phemenological model for applied-field MPD thrusters. *Acta Astronautica*, 107:177–186, 2015. doi:10.1016/j.actaastro.2014.11.017.

[10]W. J. Coogan and E. Y. Choueiri. A critical review of thrust models for applied-field magnetoplasmadynamic thrusters. In *AIAA Propulsion and Energy 2017*, AIAA-2017-4723, Atlanta, Georgia, July 10–12, 2017. doi:10.2514/6.2017-4723.

[11]V. B. Tikhonov, S. A. Semenikhin, V. A. Alexandrov, and G. A. Popov. Research of plasma acceleration processes in self-field and applied magnetic field thrusters. In *23rd International Electric Propulsion Conference*, IEPC-93-076, Seattle, WA, Sept. 13–16, 1993.

[12]V. B. Tikhonov, S. A. Semenikhin, J. R. Brophy, and J. E. Polk. Performance of 130 kW MPD thruster with an external magnetic field and Li as a propellant. In *25th International Electric Propulsion Conference*, IEPC-97-117, Cleveland, OH, Aug. 24–28, 1997.

[13]V. Kim, T. Tikhonov, and S. Semenikhin. The second quarterly report on the stages ##2A, B of the contract on the research studies no. NASW-4851 between RIAME MAI and NASA. Technical Report NASW-4851, RIAME MAI, July 1996.

[14]V. Kim, T. Tikhonov, and S. Semenikhin. The fourth quarterly (final) report on the stage ## 3 "C", "D" of the contract on the research studies no. NASW-4851 between RIAME MAI and NASA. Technical Report NASW-4851, RIAME MAI, Apr. 1997.

[15]P. J. Turchi. *The Cathode Region of a Quasi-Steady Magnetoplasmadynamic Arcjet*. PhD thesis, Princeton University, Sept. 1970.

[16]A. P. Bruckner and R. G. Jahn. Spectroscopic studies of the exhaust plume of a quasi-steady MPD accelerator. Technical Report 1041, NASA Research Grant NGL 31-001-005, 1972.

[17]R. M. Myers, A. J. Kelly, and R. G. Jahn. Energy deposition in low-power coaxial plasma thrusters. *Journal of Propulsion*, 7(5):732–739, 1991. doi:10.2514/3.23386.

[18]D. Lev. *Investigation of Efficiency in Applied Field MagnetoPlasmaDynamic Thrusters*. PhD thesis, Princeton University, Jan. 2012.

[19]R. G. Jahn. *Physics of Electric Propulsion*, chapter 8, pages 240–244. Dover Publications, Inc., Mineola, NY, 1968.

[20]W. J. Coogan, M. A. Hepler, and E. Y. Choueiri. Measurement of the applied-field component of the thrust of a lithium Lorentz force accelerator. In *52nd AIAA/SAE/ASEE Joint Propulsion Conference*, AIAA-2016-4537, Salt Lake City, UT, July 25–27, 2016. doi:10.2514/6.2016-4537.

[21]G. L. Cann, R. L. Harder, and R. A. Moore. Hall current accelerator. Technical Report NASA CR-54705/EOS 5470-Final, Electro-Optical Systems, Inc., Feb. 1966.

[22]R. R. John and S. Bennett. Final report: Arcjet technology research and development. Technical Report NASA CR-54687/RAD-TR-65-37, AVCO Corporation, NASA Contract NAS 3-5900, Dec. 1965.

[23]W. J. Coogan. AF-MPDT database. URL: http://alfven.princeton.edu/tools/afmpdt-database.

[24]R. M. Myers. Applied-field MPD thruster geometry effects. Technical Report NASA CR-187163/AIAA-91-2342, Sverdum Technology, Inc., Lewis Research Center Group, NASA Contractor Report 187163, Aug. 1991.

[25]G. L. Cann, R. A. Moore, R. L. Harder, and P. F. Jacobs. High specific impulse thermal arcjet thrustor technology part II: Performance of Hall arc jets with lithium propellant. Technical Report AFAPL-TR-65-48, Part II, Electro-Optical Systems, Inc., Jan. 1967.

[26] J. S. Sovey and M. A. Mantenieks. Performance and lifetime assessment of magnetoplasmadynamic arc thruster technology. *Journal of Propulsion*, 7(1):71–83, 1991. doi:10.2514/3.23296.

[27] G. Krülle and E. Zeyfang. Preliminary conclusions of continuous applied field electromagnetic thruster research at DFVLR. In *AIAA 11th Electric Propulsion Conference*, AIAA-75-417, New Orleans, LA, Mar. 19–21, 1975. doi:10.2514/6.1975-417.

[28] G. Krülle, M. Auweter-Kurtz, and A. Sasoh. Technology and application aspects of applied field magnetoplasmadynamic propulsion. *Journal of Propulsion*, 14(5):754–763, 1998. doi:10.2514/2.5338.